Image formation in a transmission electron microscope equipped with an environmental cell: Single-walled carbon nanotubes in source gases

H. Yoshida[1] and S. Takeda[1,2,*]

[1]*Department of Physics, Graduate School of Science, Osaka University, 1-1 Machikane-yama, Toyonaka, Osaka 560-0043, Japan*

[2]*Department of Computational Nanocharacterization, Division of Nanocharacterization, Nanoscience and Nanotechnology Center, The Institute of Scientific and Industrial Research (ISIR), Osaka University, Mohogaoka 8-1, Ibaraki, Osaka 567-0047, Japan*

(Received 20 May 2005; revised manuscript received 8 August 2005; published 23 November 2005)

We have outlined a theory of image formation in a transmission electron microscopy equipped with an environmental cell (E-TEM). We have applied the outlined theory to simulating high-resolution transmission electron microscopy (HRTEM) images of single-walled carbon nanotubes (SWNT's) in source gases of ethanol at the actual growth condition: the pressure and the temperature of ethanol gas are equal to 5 Torr and 800 °C, respectively. It is noteworthy that the growth process can be reproduced in E-TEM's. We have suggested that the diameter and chirality of SWNT's are most likely determined in a Fourier transform of HRTEM images.

DOI: 10.1103/PhysRevB.72.195428 PACS number(s): 68.37.Lp, 81.07.De, 61.46.+w, 81.15.Gh

I. INTRODUCTION

The solid-gas reaction is a fundamental process by which various materials are formed and transformed. As a recent example, single-walled carbon nanotubes (SWNT's),[1] one of the best nanomaterials for future nanotechnology, are grown at metal catalysts in source gases of proper pressure. Though the extraordinary electronic properties of SWNT's are known to be structure sensitive,[2–6] we have not yet grown SWNT's of desired structures selectively. This suggests that solid-gas reactions need to be better understood at the atomic level. A transmission electron microscope (TEM) equipped with a gas-filled specimen chamber is of particular interest in this respect. Several pioneer works have revealed various solid-gas reactions at high spatial resolution.[7–10] Nevertheless, this emerging science has never been guided by theory.

In a TEM, a gas of interest should be confined in a small specimen chamber—namely, an environmental cell (E cell).[8,9] This is definitely required, since a path of traveling electrons in a TEM should be cleared of residual gases, especially in the accelerating tube. Two types of E cells have been developed until now. In the first type, a specimen is enclosed in a container in which a gas of rather high pressure is filled or flows. A specimen is observed through both a gas and two parallel windows of the container. The windows are made of thin solid film and are transparent to electron beams to some extent. This type of E cell has been installed in higher-voltage electron microscopes. In the other type of E cell, a few sets of small orifices are arranged along the path of electrons and the parts divided by pairs of orifices are evacuated independently by additional vacuum pumps. Utilizing this differential pumping system, we can localize a gas of certain pressure only around a specimen while the other parts are evacuated fully as in a conventional TEM. The attainable pressure at a specimen reaches a few Torr even in an E cell of this type.[10] TEM's equipped with E cells are occasionally called E-TEM's.[9]

It is well known that fast electrons are scattered by gases, giving rise to distinctive electron diffraction. Analyzing the diffraction patterns based on the simple kinematical diffraction theory, we can deduce interatomic distances of a gas molecule.[11,12] In contrast, much less knowledge has been accumulated of the effect of gases on TEM images even experimentally, and the physics behind E-TEM image formation has never been considered. In this paper, we outline a theory of E-TEM image formation and apply it to simulating high-resolution (HR) TEM images of SWNT's in a source gas. We suggest that structure parameters of SWNT's are most probably determined during growth by means of E-TEM.

II. OUTLINE OF E-TEM IMAGE FORMATION

We describe a theory of image formation of a thin solid specimen in gases. First, we examine scattering objects in the two types of existing E cells in more detail. In an E cell of differential pumping type, gases fill the gap between the magnetic pole pieces of the objective lens and a specimen is immersed in the gases. The gap is usually a few millimeters. In the gap, fast electrons are scattered by gases in front of a specimen, then by the specimen, and finally by gases behind the specimen. Bores of the pole pieces are well evacuated by a differentially pumping system, so we ignore electron scattering by residual gases in the bores. In an E cell of window type, on the other hand, gases are localized only between two parallel windows several μm to mm apart. The windows are much defocused in actual observations and appear as only a blurry background in TEM images. Between the windows, electrons are scattered by both the specimen and gases as in an E cell of the other type. Therefore, we represent scattering objects in any type of E cell as a supercell in which a large number of gas molecules are distributed in addition to a thin solid specimen [Fig. 1(a)]. We assume that both temperature T and pressure P of gases are constant over a supercell, thereby estimating the number of molecules in the supercell simply by the ideal gas law.

The speed of electrons in TEM's exceeds half the speed of light, so we can safely regard gas molecules as being at rest. Based on this frozen gas model, we can calculate the wave function of the stationary scattering state of electron in prin-

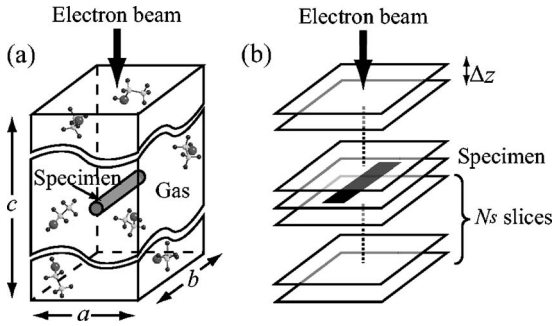

FIG. 1. Model of a thin solid specimen in gases. (a) A thin solid specimen is located at the center of a supercell. In this paper, a SWNT locates with their tube axis normal to the electron beam. Gas molecules are distributed in a supercell randomly. The cell sizes are represented by a, b, and c. (b) A supercell is divided into several slices for simulation.

ciple. However, even an electron source of field emission type emits electrons only at the rate of 10^{12} electrons per second, or an electron per 1 ps. In this interval of electron emission, even sluggish gas molecules shift greatly. For instance, the mean speed of ethanol molecules is approximately 370 m/s at room temperature, so they move by about 0.4 nm per 1 ps on average. In other words, each electron encounters a different instantaneous arrangement of molecules and the corresponding scattering events are evidently independent. Furthermore, it usually takes 0.1 to a few seconds to record a HRTEM image. During this recording time, a large number of independent scattering events are statistically averaged. Therefore, the treatment of electron scattering by gases in E-TEM has a lot in common with that by lattice vibration in crystals,[13,14] in which the time-averaged procedure enables us to simulate thermal diffuse scattering of one electron. Similarly, we calculate wave functions for a number of different arrangements of stationary molecules and simulate corresponding TEM images. Averaging these TEM images incoherently, we finally obtain an E-TEM image. We describe the actual treatment below.

After generating a random arrangement of molecules in a supercell, we simulate multiple-electron scattering in the supercell based on the multislice theory.[15] The supercell is divided into a number of thin slices which are separated by Δz along the electron beam direction [Fig. 1(b)]. We can simulate the wave amplitude at each slice sequentially along the traveling direction of electrons.[15] It is noted that the incident electron wave at the specimen, φ_0, is not a plane wave but already disturbed by gases in front of the specimen. The electron wave at the exit surface of the supercell, φ^{g} is described as

$$\varphi^{\mathrm{g}} = q^{\mathrm{g}}_{N_s}\Big[\cdots\Big[q^{\mathrm{g}}_{2}\Big[q^{\mathrm{g}}_{1}\Big[\Big[q^{\mathrm{sp}}\varphi_0\Big]_0 * p(\Delta z)\Big]_1 * p(\Delta z)\Big]_2\cdots\Big]_{N_s} * p(\Delta z) \tag{1}$$

in which q^{sp}, q^{g}_i $(i=1,2,\ldots,N_s)$, $p(\Delta z)$, and $*$ represent the transmission function of the specimen, transmission functions of ith slices of gases in the rear side of the specimen, the propagation function of Fresnel diffraction through the distance Δz, and convolution integral, respectively. Here, N_s is the number of slices in the rear side of the specimen [Fig. 1(b)].

The electron wave is further disturbed by the spherical and chromatic aberrations and the defocus of the objective lens. In conventional TEM, we impose these disturbances on the electron wave at the electron exit surface of a specimen via the contrast transfer function (CTF).[16,17] In E-TEM, gases are immersed in the objective lens. Change in the refractive index is, however, negligible; for instance, a methanol gas ($P=5$ Torr, $T=300$ K) which fills the gap 5 mm thick corresponds to solid carbon only about 20 nm thick. Furthermore, gases, spread in the objective lens homogeneously, cause no directional effect on propagating electron waves. Also, we safely ignore the energy dispersion of electrons in the thin gases. Therefore, the aberrations can be imposed on φ^{g} in Eq. (1) via the conventional CTF. Defocus in the CTF needs correcting, since φ^{g} in Eq. (1) represents an electron wave which propagates from a specimen toward the objective lens by distance $(N_s+1)\Delta z$ [see Fig. 1(b)]. Defining the amount of defocus Δf conventionally as the distance from the electron exit surface of a specimen to the plane conjugate to the viewing plane of image, we must offset the amount of defocus in the CTF, Δf_{CTF}, as follows:

$$\Delta f = \Delta f_{\mathrm{CTF}} + (N_s + 1)\Delta z, \tag{2}$$

in which the sign of Δf is defined negative at underdefocus. In this way, we compute an instantaneous image intensity.

We iterate the procedure for different random arrangements of molecules, as is mentioned above. In the iteration, the specimen remains at the same position in supercells. Averaging the instantaneous image intensity I_i $(i=1,2,\ldots,N_a)$ in the simple formula

$$I = \frac{1}{N_a}\sum_{i=1}^{N_a} I_i, \tag{3}$$

we finally obtain an E-TEM image intensity, in which N_a is the number of iterations. We can compute electron diffraction in a similar way, by averaging the intensity of instantaneous diffraction patterns.

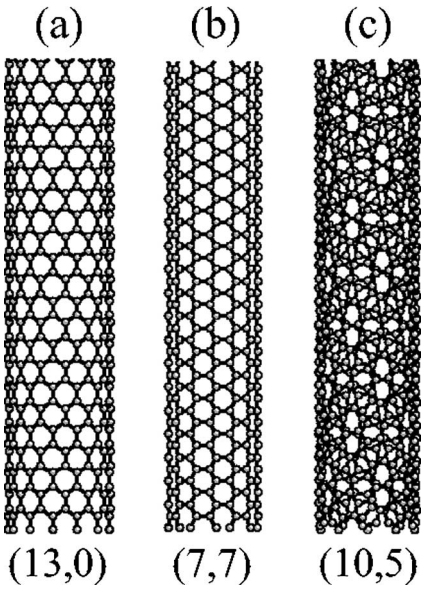

FIG. 2. Three kinds of SWNT's. (a) (13,0) SWNT of zigzag type, $d=1.02$ nm, (b) (7,7) SWNT of armchair type, $d=0.95$ nm, and (c) (10,5) SWNT of chiral type, $d=1.04$ nm. SWNT's in (a) and (c) are known to be semiconductors, while the one in (b) is known to be metal.

III. STRUCTURAL PROPERTY AND GROWTH OF SWNT'S

SWNT's are cylindrical forms of carbon in which carbon atoms are bonded mostly via sp^2 hybridization and therefore form six-membered atomic rings.[1] We can reproduce this structure formally by rolling up a single layer of graphite, though the actual growth process of SWNT's has remained unclear at the atomistic level. It is known that the structures of SWNT's are varied greatly, somewhat corresponding to various ways of rolling up a single layer of graphite. Each structural variant of the SWNT can be described fully by a set of parameters—i.e., the diameter d and the chiral angle θ or the chiral index (n,m)[2]. Structural variants can be identified by HRTEM images,[18] their Fourier transforms (FT's),[18] and electron diffraction.[19,20] More importantly, each structural variant behaves variously as metals and semiconductors.[2–4] For instance, SWNT's exhibit metallic properties when $n-m=3l$ (l: integers). Three typical SWNT's of about 1.0 nm in diameter such as the zigzag type (13,0), the armchair type (7,7), and the chiral type (10,5) are shown in Fig. 2. The first and third ones are semiconductors, while the second one is known to be metal. For applying SWNT's to electronic devices more effectively, it is crucial to grow SWNT's of desired properties selectively.

SWNT's are synthesized by arc discharge,[1,21] laser ablation,[22] and chemical vapor deposition (CVD).[23–25] Among these processes, CVD has been studied most extensively. Preparing nanocatalysts of desired sizes at desired sites on a substrate for CVD, we probably control the nucleation sites and the radius of SWNT's. Nevertheless, even the diameter of SWNT's has not yet been controlled precisely. *In situ* E-TEM is needed to reveal the actual CVD process of SWNT's at the atomic level.

IV. IMAGE SIMULATION OF SWNT's IN SOURCE GASES

A. Parameters for simulation

We locate a SWNT in a supercell with its tube axis normal to the incident electron beam (Fig. 1). The supercells arrange periodically in the lateral directions or normal to the electron beam according to the algorithm of image simulation. The lateral dimension of a supercell should be sufficiently larger than a specimen in order to suppress false interference over supercells which may distort images of a specimen. As discussed in the Appendix, we chose the lateral dimension of $a=b=8$ nm which is twice the length of SWNT's—i.e., 4.8 nm.

We select ethanol (C_2H_5OH) as a source gas. The pressure of ethanol gases for growing SWNT's is lower than that of the other kinds of source gases such as methane: it is lower than 5 Torr in the temperature range from 600 to 800 °C.[25] This CVD environment may be reproduced in existing E-TEM's. In simulations, we vary P from 0 to 5 Torr while T is set constant at 800 °C. Assuming the thickness of a supercell, c, to be 3 mm at this moment, we estimate the number of ethanol molecules in the supercell, N, by the ideal gas law $N=N_0\times PV/RT$, where V, N_0, and R are the volume of the supercell ($V=abc=8$ nm$\times 8$ nm$\times 3$ mm), the Avogadro constant, and the gas constant, respectively. For instance, N at $P=5$ Torr is equal to 8600. We arrange N ethanol molecules[26] randomly in a supercell both translationally and rotationally, as depicted in Fig. 1(a). In order to accomplish image simulation within reasonable computing times, we reduce the thickness c and compress the gas accordingly. We assume here that $c=100$ nm. We are aware that the artificial compression is somewhat rough. However, as shown in the Appendix, the essential features of images are well reproduced with supercells 100 nm thick. The supercell is then divided into 100 slices, as shown in Fig. 1(b). A SWNT is projected on the central slice while randomly arranged molecules are projected on the other 99 slices.

Parameters of electron optics in our simulation are similar to those of existing 200-kV TEM's equipped with a field emission gun: accelerating voltage of 200 kV (electron wave length, $\lambda=0.00251$ nm), the spherical aberration coefficient of the objective lens of 1.2 mm, the chromatic aberration coefficient of the objective lens of 1.2 mm, and the radius of the objective aperture of 7.1 nm^{-1}. The Scherzer defocus Δf_{Sch} is estimated to be $-\sqrt{4C_s\lambda/3}=-63.4$ nm. As is well known, the characteristic electron diffraction of SWNT's appears around 4.7 nm^{-1} in the reciprocal space. The diffraction contributes to HRTEM images out of phase at the Scherzer defocus in standard 100–200-kV HRTEM's. However, it was recently shown[18] that, at the optimum defocus which is slightly deviated from the Scherzer defocus, the characteristic diffraction can be included in-phase as well as other diffraction at lower scattering angles. Accordingly, characteristic moiré fringe of SWNT's appears clearly in HRTEM images. We simulate TEM images mostly at this optimum defocus Δf_{opt}, which is estimated to be −57.4 nm according to the present parameters of electron optics. We assume the standard deviation of mechanical vibration on the lateral plane to be 0.1 nm. The intensity of HRTEM images

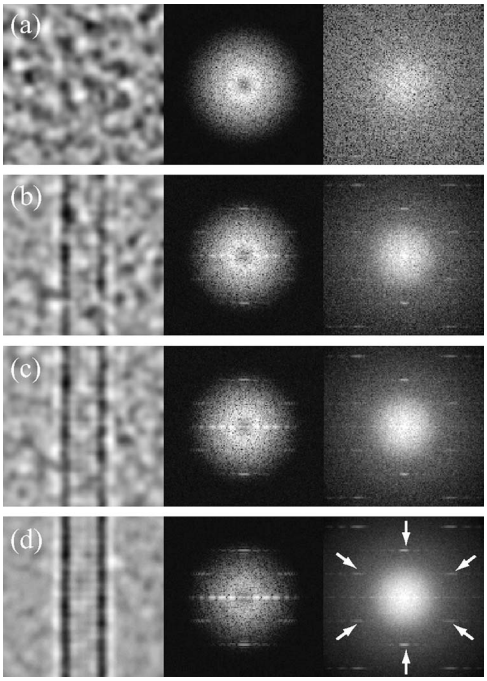

FIG. 3. Effect of averaging in HRTEM images and electron diffraction patterns. HRTEM images in the left column, FT's in the central column, and simulated electron diffraction patterns in the right column. (a) $N_a=1$, (b) $N_a=10$, (c) $N_a=20$, and (d) $N_a=100$. The characteristic diffraction of SWNT's around 4.7 nm^{-1} is indicated by arrows in (d). (13,0) SWNT, $P=5$ Torr, $\Delta f=\Delta f_{opt}$.

is simulated on 512×512 pixels with an accuracy of 10^{-8}, and the central areas of 256×256 pixels are presented with a depth of 8 bits. The intensity of FT's of HRTEM images and that of simulated diffraction patterns are shown in logarithm scaling. Only in a standard procedure of TEM image simulation do we utilize the MACTEMPAS software conveniently (Total Resolutions, CA, USA).

B. Validity of E-TEM image simulation

In order to simulate a realistic E-TEM image, the number of iteration, N_a, should be large. In an instantaneous image ($N_a=1$), a SWNT is almost covered behind false granular contrast and the characteristic diffraction of SWNT is smeared out, as seen in Fig. 3(a). Ethanol gas in the supercell roughly corresponds to amorphous carbon 6 nm thick, and the image in Fig. 3(a) is somewhat similar to that of a SWNT supported on an amorphous carbon film.[27] When we average instantaneous images several times, then the contrast of gases becomes smoother and moiré fringe of SWNT's appears clearly, as shown in Figs. 3(b)–3(d). The false granular contrast mostly disappears when 100 instantaneous images are averaged [Fig. 3(d)]. In simulated electron diffraction in Figs. 3(b)–3(d), the characteristic diffraction is well reproduced as well as halo due to ethanol molecules. Clearly, the characteristic diffraction can be also seen in FT's of HRTEM images when $N_a\geqslant10$. We think that, as demonstrated in Figs. 3(b)–3(d), averaging is practically sufficient whenever N_a exceeds 10 within the framework of the present treatment.

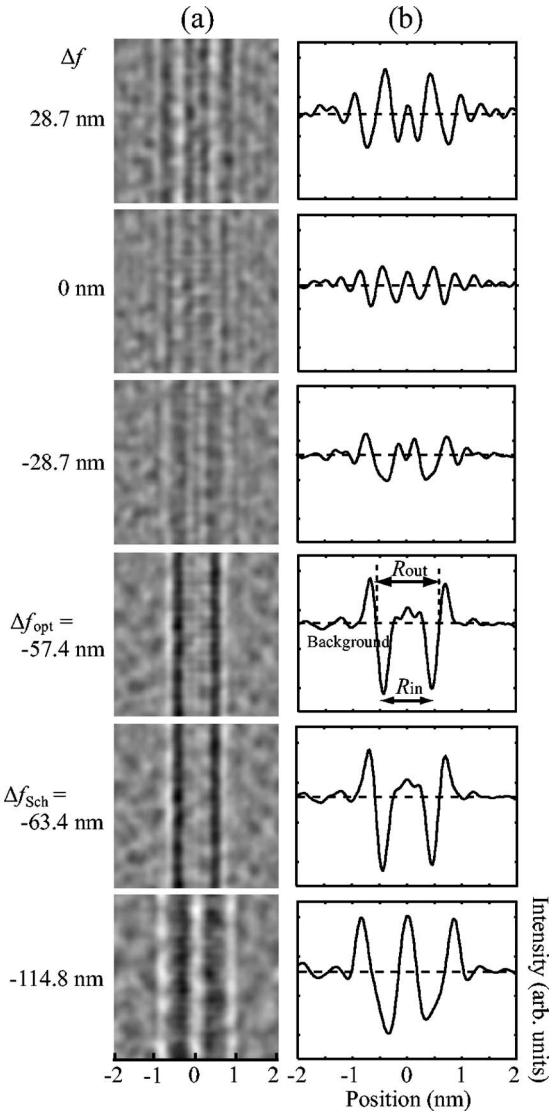

FIG. 4. (a) Simulated through-focus HRTEM images and (b) corresponding projected intensity profiles. Defocus Δf is indicated in figures. (13,0) SWNT, $P=1$ Torr, $N_a=10$.

C. Determination of the diameters of SWNT's in gases

We examine the possibility of determining the diameter of SWNT's in gases. Figure 4(a) shows through-focus HRTEM images. A pair of dark and white lines appears in each side of the SWNT in the range of underdefocus, $\Delta f\leqslant-57.4$ nm. At the Scherzer defocus ($\Delta f_{Sch}=-63.4$ nm), the dark lines appear the clearest. With the increase of underdefocus, the dark and white lines become broader and more blurry. Averaging the image intensity along the tube axis, we obtain the projected intensity profiles [Fig. 4(b)]. In the intensity profiles, we first define the distance between the two dark lines as R_{in}. It was reported that R_{in} at the Scherzer defocus is 10% smaller than the actual diameter of SWNT's when the diameter is larger than 1.0 nm.[28] Similarly, R_{in} estimated in gases is about 10% smaller than the actual diameter. The difference becomes larger as Δf deviates from the Scherzer defocus. This discrepancy is accounted for by image delocalization, or Fresnel diffraction, which is strongly defocus dependent. It is

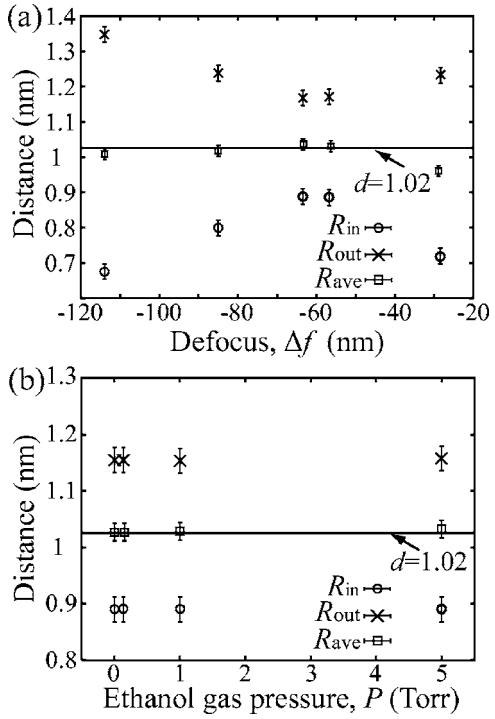

FIG. 5. R_{in}, R_{out}, and R_{ave} are shown (a) as a function of defocus, Δf ($P=1$ Torr) and (b) as a function of the pressure of ethanol gases, P ($\Delta f=\Delta f_{Sch}$). (13,0) SWNT, $d=1.02$ nm, $N_a=10$.

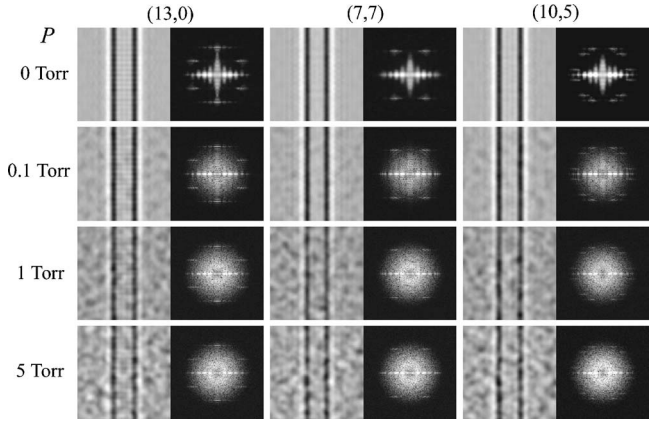

FIG. 6. Simulated HRTEM images of three kinds of SWNT's in an ethanol gas of different pressures. Corresponding FT's are shown in the right. $\Delta f=\Delta f_{opt}$. $N_a=10$ for all the simulated HRTEM images except those at 5 Torr in which $N_a=30$.

also noted that the projected electrostatic potential of a SWNT does not reach the maximum at the outermost atoms. We next see the middle point between a pair of white and dark lines, at which the intensity is equal to the background. Accordingly, we define R_{out} as the distance between the two middle points and R_{ave} as the average of R_{in} and R_{out}, as indicated in Fig. 4(b). In Fig. 5(a), R_{in}, R_{out}, and R_{ave} are plotted as a function of Δf. R_{in} and R_{out} change reversely, and R_{ave} stays close to the actual diameter independently of defocus. It is also shown that R_{ave} is in good agreement with the actual diameter up to 5 Torr, as shown in Fig. 5(b). This holds in the three kinds of SWNT's in our simulation. Therefore, measuring R_{ave}, we most probably determine the diameter of SWNT's in gases accurately.

D. Chirality of SWNT's

We now examine detail HRTEM images. It is recently claimed[18] that the chirality of SWNT's can be determined in vacuum by HRTEM. In the study, HRTEM images are recorded at the optimum defocus Δf_{opt}. In through-focus images in Fig. 4(a), the moiré fringe that represents the chirality is the clearest at Δf_{opt} even in gases. We have simulated HRTEM images of three kinds of SWNT's in gases at Δf_{opt} (Fig. 6). In vacuum ($P=0$ Torr) and gases of lower pressures, we can identify SWNT's in both HRTEM images and their FT's. With the increase of gas pressure, images are gradually blurred. Nevertheless, we can see moiré fringe in SWNT of zigzag type (13,0) up to 5 Torr. For SWNT's of the other types, moiré fringes are very blurred at 5 Torr. However, the characteristic diffraction of all the structural variants are well reproduced in FT's even at 5 Torr clearly. The intensity maximum of the characteristic diffraction remains at the same position at any gas pressure. As mentioned in Sec. IV A, SWNT's can be synthesized well in an ethanol gas of 5 Torr. Therefore, in our conclusion, three types of SWNT's can be distinguished in the actual CVD process. It is also possible to determine the chirality of SWNT's to some extent.

E. Remarks on experimental high-resolution E-TEM of SWNT's

We have assumed so far that the electron beam direction is normal to the tube axis. However, such a case may be unusual in actual observation: SWNT's are tilted more or less toward the electron beam. We have confirmed that the distance between maxima of characteristic diffraction decreases as the tilting angle increases, and they coalesce at large tilting angles. Nevertheless, as long as the maxima are visible, it is likely to deduce chirality according to the previous work.[19]

Growth of multiwalled carbon nanotubes[29] and SWNT's[30] has already been observed by means of E-TEM, and some interesting features on the growth of nanotubes has been revealed with resolution attainable in existing E-TEM's. As in the study in Ref. 29, higher accelerating voltage of electrons such as 300 kV is usually preferred for E-TEM's, since higher penetrating power is needed to observe a specimen through gases. However, higher-energy electrons cause electron-irradiation damages severely. In fact, it seems that[18] the proper accelerating voltage is around 120 kV for observing HRTEM images of SWNT's in vacuum. Also, lower-energy electrons seem more suitable to recording HRTEM images of carbon with high sensitivity. We do not intend to draw any definite conclusion on the proper accelerating voltage on this subject, and we chose the medium voltage of 200 kV (Ref. 30) for simulations in this paper.

In actual observations, mechanical vibrations of SWNT's may also disturb HRTEM images severely. This is inevitably caused by the vibration of a specimen holder and SWNT's

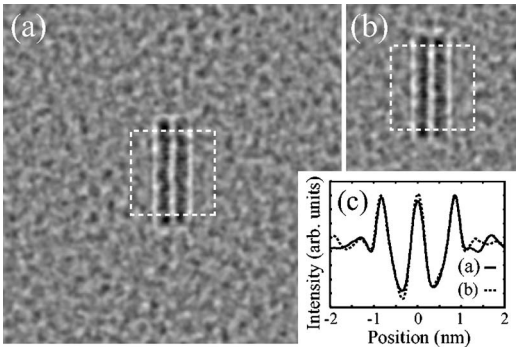

FIG. 7. Influence of the lateral dimension of the supercell on simulated HRTEM images. Defocus Δf is equal to -114.8 nm where delocalization appears clearly. The lateral dimension is (a) $a=b=16$ nm and (b) $a=b=8$ nm. (c) Projected intensity profiles of the center area of (a) and (b) are indicated by solid and dotted lines, respectively. (13,0) SWNT, $P=1$ Torr, $N_a=10$.

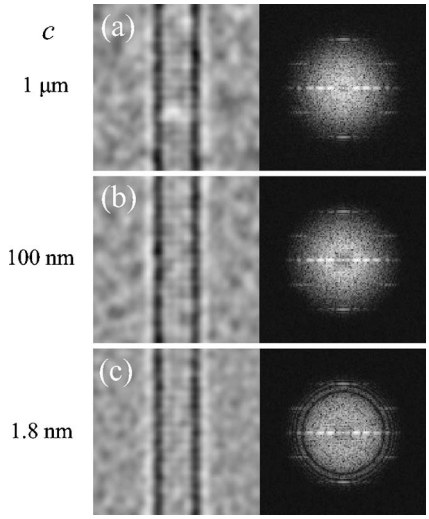

FIG. 8. Simulated HRTEM images with the supercell of various thickness and the corresponding FT's. The thickness c is equal to (a) 1 μm, (b) 100 nm, or (c) 1.8 nm. (13,0) SWNT, $P=1$ Torr, $N_a=10$, $\Delta f=\Delta f_{\mathrm{opt}}$.

themselves, the poor support of SWNT's on a substrate even in a conventional TEM. Suppose the amplitude of lateral vibrations of SWNT's exceeds the interval of moiré fringes of SWNT's—i.e., about 0.2 nm—the structural features of SWNT's cannot be revealed. As is recently shown,[18] the moiré fringes are observable in relatively stationary SWNT's. Therefore, we simulate HRTEM images of stationary SWNT's, assuming the amplitude of lateral vibration to be 0.1 nm, as described in Sec. IV A. In addition, SWNT's probably vibrate along the electron beam direction with the similar amplitude as lateral vibration. This vertical vibration causes defocus spread effectively. This defocus spread is, however, much smaller than that due to the chromatic aberration of the objective lens—i.e., several tens of nanometers—so we ignore the vertical vibration of SWNT's in our simulation. In E-TEM's, the flow of gases may cause additional vibration of SWNT's. Therefore, the technical challenge to suppressing the vibration and the damages in E-TEM's may be very important in order to reproduce experimentally the details of simulated HRTEM images as predicted in this study. Moreover, SWNT's are occasionally kinked and include structural defects. These defective structures naturally affect HRTEM images and prevent us from identifying the basic structural features such as chirality and diameter. However, straight and less defective SWNT's frequently grow whenever the growth condition is well controlled. Therefore, we consider that image simulation of SWNT's in this paper is a useful guide to experimental E-TEM.

V. CONCLUSIONS

We have outlined a theory of E-TEM image formation and applied it to simulating HRTEM images of SWNT's in source gases. Since the discovery of carbon nanotubes and SWNT's, interesting properties of them have been predicted by computer simulations in various aspects.[2–4,31–33] In this paper, we have suggested that *in situ* high-resolution E-TEM can clarify the growth mechanism of SWNT's at atomic level, through which the control of diameter and chirality of SWNT's is probably made possible and therefore SWNT's can be utilized much more effectively for future nanoelectronics.

ACKNOWLEDGMENTS

The authors are indebted to Yoshikazu Homma who has conducted us to this study and Hideo Kohno for useful suggestions. The authors are also thankful to Renu Sharma for discussion on E-TEM. This work was supported by CREST of JST.

APPENDIX

We provide proofs that our simulated results are independent of the chosen supercell's size. As is well known, delocalization of HRTEM images depends strongly on defocus. When the delocalization exceeds the lateral dimension of the supercell, simulated results are distorted and incorrect. Therefore, the choice of the lateral dimension of the supercell is essential for HRTEM image simulation. In this paper, we have used the supercell with lateral dimension $a=b=8$ nm. In order to confirm the validity of this size, we have simulated HRTEM images with the supercell of larger lateral dimension $a=b=16$ nm. There is no clear difference between the images of the larger [Fig. 7(a)] and the smaller [Fig. 7(b)] supercells. As is shown in Fig. 7(c), projected intensity profiles along the tube axis in the central part of Figs. 7(a) and 7(b) are slightly different, since the arrangements of ethanol molecules are different in these supercells. However, R_{in} and R_{out}, defined in Fig. 4, are almost the same value. Therefore, the results of our simulation are independent of the chosen lateral dimension of the supercell.

We chose $c=100$ nm as the thickness of supercells. In

order to confirm the validity of this thickness, we compute HRTEM images with thicker ($c=1$ μm) and thinner ($c=1.8$ nm) supercells. As shown in Figs. 8(a) and 8(b), our supercell ($c=100$ nm) leads to similar HRTEM images and corresponding FT's of the thicker supercell. When we reduce thickness too much ($c=1.8$ nm), then a number of rings appear in FT's of simulated HRTEM images as shown in Fig. 8(c). As is well known, a thin amorphous film exhibits similar rings, called Thon rings, the radii of which systematically depend on defocus via CTF.[34] As is easily understood, gases which extend considerably along the electron beam direction never give rise to Thon rings. Therefore, a model supercell 100 nm thick in this paper is proper for HRTEM image simulation of SWNT's in the gases.

*Electronic address: takeda@tem.phys.sci.osaka-u.ac.jp

[1] S. Iijima and T. Ichihashi, Nature (London) **363**, 603 (1993).
[2] N. Hamada, S. I. Sawada, and A. Oshiyama, Phys. Rev. Lett. **68**, 1579 (1992).
[3] R. Saito, M. Fujita, G. Dresselhaus, and M. S. Dresselhaus, Appl. Phys. Lett. **60**, 2204 (1992).
[4] J. W. Mintmire, B. I. Dunlap, and C. T. White, Phys. Rev. Lett. **68**, 631 (1992).
[5] B. W. Smith, M. Monthioux, and D. E. Luzzi, Nature (London) **396**, 323 (1998).
[6] R. R. Meyer, J. Sloan, R. E. Dunin-Borkowski, A. I. Kirkland, M. C. Novotny, S. R. Bailey, J. L. Hutchison, and M. L. H. Green, Science **289**, 1324 (2000).
[7] H. Hashimoto, T. Naiki, T. Eto, and K. Fujiwara, Jpn. J. Appl. Phys. **7**, 946 (1968).
[8] H. M. Flower, J. Microsc. **97**, 171 (1972).
[9] E. D. Boyes and P. L. Gai, Ultramicroscopy **67**, 219 (1997).
[10] P. L. Hansen, J. B. Wagner, S. Helveg, J. R. Rostrup-Nielsen, B. S. Clausen, and H. Topsøe, Science **295**, 2053 (2002).
[11] M. Nakata, K. Kohata, T. Fukuyama, and K. Kuchitsu, J. Mol. Spectrosc. **83**, 105 (1980).
[12] J. Farges, M. F. de Feraudy, B. Raoult, and G. Torchet, J. Chem. Phys. **78**, 5067 (1983).
[13] Z. L. Wang, *Elastic and Inelastic Scattering in Electron Diffraction and Imaging* (Plenum, New York, 1995).
[14] C. R. Hall and P. B. Hirsch, Proc. R. Soc. London, Ser. A **286**, 158 (1965).
[15] J. M. Cowley and A. F. Moodie, Acta Crystallogr. **10**, 609 (1957).
[16] K. Ishizuka, Ultramicroscopy **5**, 55 (1980).
[17] P. G. Self and M. A. O'keefe, in *High-Resolution Transmission Electron Microscopy and Associated Techniques*, edited by P. Buseck, J. Cowley, and L. Eyring (Oxford University Press, New York, 1988), Chap. 8.
[18] A. Hashimoto, K. Suenaga, A. Gloter, K. Urita, and S. Iijima, Nature (London) **430**, 870 (2004).
[19] M. Gao, J. M. Zuo, R. D. Twesten, I. Petrov, L. A. Nagahara, and R. Zhang, Appl. Phys. Lett. **82**, 2703 (2003).
[20] J. M. Zuo, I. Vartanyants, M. Gao, R. Zhang, and L. A. Nagahara, Science **300**, 1419 (2003).
[21] C. Journet, W. K. Maser, P. Bernier, A. Loiseau, M. L. de la Chapell, S. Lefrant, P. Deniard, R. Lee, and J. E. Fischer, Nature (London) **388**, 756 (1997).
[22] A. Thess *et al.*, Science **273**, 483 (1996).
[23] H. Dai, A. G. Rinzler, P. Nikolaev, A. Thess, D. T. Colbert, and R. E. Smalley, Chem. Phys. Lett. **260**, 471 (1996).
[24] J.-F. Colomer, C. Stephan, S. Lefrant, G. V. Tendeloo, I. Willems, Z. Kónya, A. Fonseca, C. Laurent, and J. B. Nagy, Chem. Phys. Lett. **317**, 83 (2000).
[25] S. Maruyama, R. Kojima, Y. Miyauchi, S. Chiashi, and M. Kohno, Chem. Phys. Lett. **360**, 229 (2002).
[26] Y. Sawada, M. Takano, and T. Satoh, J. Mol. Spectrosc. **38**, 33 (1971).
[27] L. C. Qin, X. Zhao, K. Hirahara, Y. Ando, and S. Iijima, Chem. Phys. Lett. **349**, 389 (2001).
[28] C. Qin and L.-M. Peng, Phys. Rev. B **65**, 155431 (2002).
[29] S. Helveg, C. López-Cartes, J. Sehested, P. L. Hansen, B. S. Clausen, J. R. Rostrup-Nielsen, F. Ablid-Pedersen, and J. K. Nørskov, Nature (London) **427**, 426 (2004).
[30] R. Sharma and Z. Iqbal, Appl. Phys. Lett. **84**, 990 (2004).
[31] H. Ajiki and T. Ando, J. Phys. Soc. Jpn. **62**, 1255 (1993).
[32] W. Tian and S. Datta, Phys. Rev. B **49**, 5097 (1994).
[33] L. Chico, L. X. Benedict, S. G. Louie, and M. L. Cohen, Phys. Rev. B **54**, 2600 (1996).
[34] D. B. Williams and C. B. Carter, *Transmission Electron Microscopy* (Plenum, New York, 1996).